

Atom chip based generation of entanglement for quantum metrology

Max F. Riedel,^{1,2} Pascal Böhi,^{1,2} Yun Li,^{3,4} Theodor W. Hänsch,^{1,2} Alice Sinatra,^{3,*} and Philipp Treutlein^{1,2,5,†}

¹*Fakultät für Physik, Ludwig-Maximilians-Universität, Schellingstraße 4, 80799 München, Germany*

²*Max-Planck-Institut für Quantenoptik, Hans-Kopfermann-Straße 1, 85748 Garching, Germany*

³*Laboratoire Kastler Brossel, ENS, 24 rue Lhomond, F-75005 Paris, France*

⁴*State Key Laboratory of Precision Spectroscopy, Department of Physics, East China Normal University, Shanghai 200062, China*

⁵*Departement Physik, Universität Basel, Klingelbergstraße 82, CH-4056 Basel, Switzerland*

(Dated: May 28, 2018)

Atom chips provide a versatile ‘quantum laboratory on a microchip’ for experiments with ultracold atomic gases [1]. They have been used in experiments on diverse topics such as low-dimensional quantum gases [2], cavity quantum electrodynamics [3], atom-surface interactions [4, 5], and chip-based atomic clocks [6] and interferometers [7, 8]. A severe limitation of atom chips, however, is that techniques to control atomic interactions and to generate entanglement have not been experimentally available so far. Such techniques enable chip-based studies of entangled many-body systems and are a key prerequisite for atom chip applications in quantum simulations [9], quantum information processing [10], and quantum metrology [11]. Here we report experiments where we generate multi-particle entanglement on an atom chip by controlling elastic collisional interactions with a state-dependent potential [12]. We employ this technique to generate spin-squeezed states of a two-component Bose-Einstein condensate [13] and show that they are useful for quantum metrology. The observed -3.7 ± 0.4 dB reduction in spin noise combined with the spin coherence imply four-partite entanglement between the condensate atoms [14] and could be used to improve an interferometric measurement by -2.5 ± 0.6 dB over the standard quantum limit [15]. Our data show good agreement with a dynamical multi-mode simulation [16] and allow us to reconstruct the Wigner function [17] of the spin-squeezed condensate. The techniques demonstrated here could be directly applied in chip-based atomic clocks which are currently being set up [18].

In the currently emerging field of quantum metrology [11], multi-particle entangled states such as spin-squeezed states [19–21] are investigated as a means to improve measurement precision beyond the ‘standard quantum limit’ [15]. This limit arises from the quantum noise inherent in measurements on a finite number of uncorrelated particles and limits today’s best atomic clocks [22]. Atom chips combine exquisite coherent control with a compact and robust setup [23], suggesting their use

for quantum metrology with portable atomic clocks and interferometers. Several techniques to create entangled states on atom chips have been proposed [16, 24–27], but none has been experimentally realized so far.

The ‘one-axis twisting’ scheme of [28] in principle allows to create a huge amount of entanglement in a two-component Bose-Einstein condensate (BEC) [13, 16, 29]. In this scheme, an initially separable (non-entangled) state, where each atom is in a superposition of two internal states $|0\rangle$ and $|1\rangle$, dynamically evolves into a spin-squeezed state in which the condensate atoms are entangled. This is due to atomic interactions that provide a nonlinear term in the Hamiltonian for the BEC internal state. In the experiments reported here, we realize this scheme on an atom chip. A notable feature is that we control the interactions through the wave function overlap of the two states [16, 30] in a state-dependent microwave potential [12]. This is a new and versatile technique for tuning of interactions in a BEC which also works in magnetic traps and for atomic state pairs where no convenient Feshbach resonances exist. We use such a pair, the hyperfine states $|0\rangle \equiv |F=1, m_F=-1\rangle$ and $|1\rangle \equiv |F=2, m_F=1\rangle$ of ^{87}Rb , which is also employed in chip-based atomic clocks with magnetically trapped atoms [6, 18].

A two-mode model [16] provides a starting point to understand how squeezing is created in our experiment. The internal state of a BEC of N two-level atoms can be described by a collective spin $\mathbf{S} = \sum_{i=1}^N \mathbf{s}_i$, the sum of the individual spins $1/2$ of each atom (see Fig. 1a). Its component $S_z = (N_1 - N_0)/2$ is half the atom number difference between the states and thus directly measurable. A $\pi/2$ -pulse applied to a BEC in $|0\rangle^{\otimes N}$ prepares it in a coherent spin state $(|0\rangle + |1\rangle)^{\otimes N}/2^{N/2}$ with mean spin $\langle S_x \rangle = N/2$ and $\langle S_y \rangle = \langle S_z \rangle = 0$. This is a product state in which the atoms are uncorrelated and the quantum noise is evenly distributed among the spin components orthogonal to the mean spin, $\Delta S_y^2 = \Delta S_z^2 = N/4$, satisfying the Heisenberg uncertainty relation $\Delta S_y \Delta S_z = |\langle S_x \rangle|/2$. This noise gives rise to the standard quantum limit if the state is used in a Ramsey interferometer such as an atomic clock [22].

Quantum correlations between the atoms can reduce the variance of one spin quadrature in the yz plane at

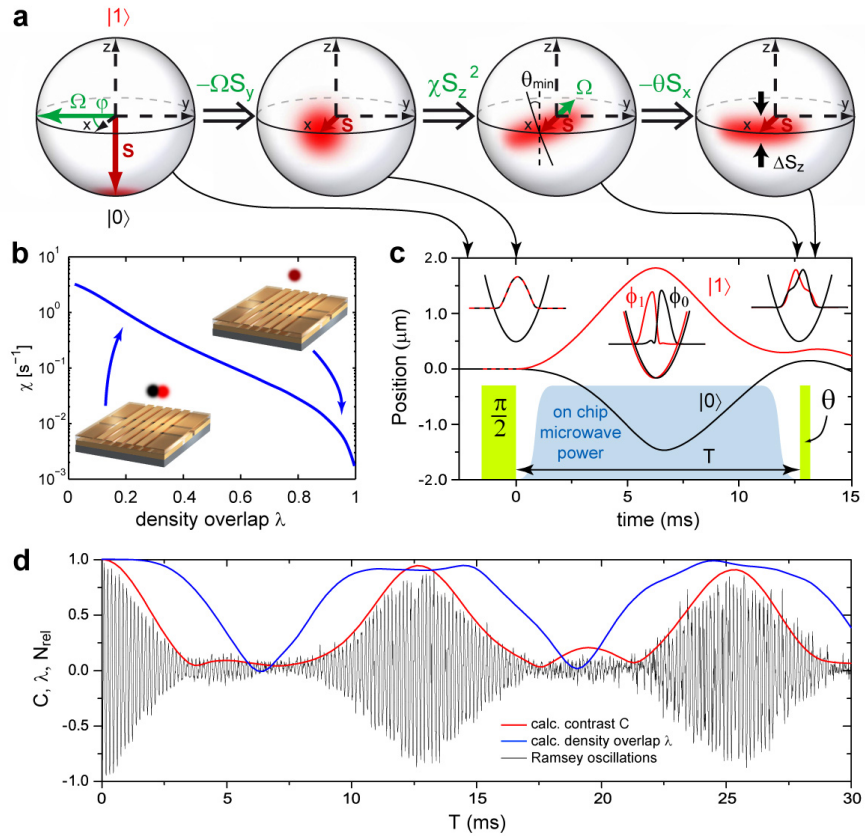


FIG. 1: **Spin squeezing and entanglement through controlled interactions on an atom chip.** **a**, Evolution of the BEC internal state on the Bloch sphere ($\delta = 0$ for illustration). Starting with all atoms in $|0\rangle$, a $\pi/2$ -pulse prepares a coherent spin state with mean spin $\langle \mathbf{S} \rangle$ along x and isotropic quantum noise in the yz -plane (fuzzy red circle). Subsequent nonlinear evolution with χS_z^2 deforms the noise circle into an ellipse, creating a spin-squeezed state with reduced noise at an angle θ_{\min} . For state tomography, a second pulse rotates the state around $-x$ by a variable angle θ , followed by detection of S_z . **b**, Control of the nonlinearity χ on the atom chip. χ depends on the difference of intra- and inter-state atomic interactions. Its dependence on the normalized density overlap λ of the two BEC components is shown, calculated from stationary mode functions in potentials of increasing separation. **c**, Experimental sequence and motion of the two BEC components corresponding to **a**. In between the pulses for internal-state manipulation (green), a state-dependent microwave potential is turned on (blue; pulse durations and microwave ramp times exaggerated for clarity). It dynamically splits and recombines the two BEC components, so that $\chi > 0$ during the time T . The simulated center-of-mass motion of the two states $|0\rangle$ (black) and $|1\rangle$ (red) is shown as a function of time. A slightly asymmetric splitting of the potentials results in an asymmetric oscillation. Insets: corresponding BEC mode functions ϕ_0 and ϕ_1 along the splitting direction at the beginning, in the middle, and at the end of the sequence. **d**, Measured Ramsey fringes in the normalized population difference N_{rel} (here, $\theta = \pi/2$). Between the pulses, δ is nonzero (see Supplementary Information), resulting in spin precession. The splitting and recombination of the BEC modulates the fringe contrast. Here, T is scanned beyond the duration of the sequence in **a**+**c**, so that up to ~ 2.5 oscillations are induced. The simulated contrast C (red) and density overlap λ (blue) are shown for comparison.

the cost of increasing the variance of the orthogonal one, resulting in a spin-squeezed state [28]. To quantify its usefulness for metrology, one introduces the squeezing parameter [15] $\xi^2 = N \Delta S_{\theta, \min}^2 / \langle S_x \rangle^2$, where $\Delta S_{\theta, \min}^2$ is the minimal variance of the spin in the yz plane (see Fig. 1a). The normalization by $\langle S_x \rangle^2$ takes into account that improving interferometric sensitivity requires not only reducing noise but also maintaining high interferometer contrast $C = 2|\langle S_x \rangle|/N$. A state with $\xi^2 < 1$ allows one to overcome the standard quantum limit in a Ramsey interferometer by a factor ξ with respect to the use of an uncorrelated ensemble of atoms [15]. Fur-

thermore, ξ^2 is an entanglement witness, with $\xi^2 < 1$ indicating at least bipartite entanglement between the condensate atoms [13].

We produce spin-squeezed states by means of time evolution through the ‘one-axis twisting’ Hamiltonian [28]:

$$H/\hbar = \delta S_z + \Omega S_\varphi + \chi S_z^2, \quad (1)$$

which describes our BEC in good approximation [16]. The first term in (1) describes spin precession around z at the detuning δ . The second term describes spin rotations around an axis $S_\varphi = (\cos \varphi) S_x - (\sin \varphi) S_y$ due to a coupling of $|0\rangle$ and $|1\rangle$ with Rabi frequency Ω and phase

φ . The third, nonlinear term of strength χ arises due to elastic collisional interactions in the BEC. It ‘twists’ the state on the Bloch sphere (see Fig. 1a), resulting in spin squeezing and entanglement.

An essential feature of our experiment is the control of this nonlinearity. Its coefficient

$$\chi = \frac{1}{2\hbar} (\partial_{N_0}\mu_0 + \partial_{N_1}\mu_1 - \partial_{N_1}\mu_0 - \partial_{N_0}\mu_1)_{\langle N_0 \rangle, \langle N_1 \rangle} \quad (2)$$

depends on derivatives of the chemical potentials

$$\mu_j = \langle \phi_j | h_j | \phi_j \rangle + \sum_{k=0,1} g_{jk} N_k \int dr^3 |\phi_j|^2 |\phi_k|^2 \quad (3)$$

of the two BEC components evaluated at the mean atom numbers $\langle N_0 \rangle = \langle N_1 \rangle = N/2$ after the $\pi/2$ -pulse. Here, h_j is the single-particle Hamiltonian including kinetic energy and the trapping potential, and $\phi_j(\mathbf{r})$ is the spatial mode function of state $|j\rangle$. The interaction strength $g_{jk} = 4\pi\hbar^2 a_{jk}/m$ between atoms in $|j\rangle$ and $|k\rangle$ depends on the corresponding s-wave scattering length a_{jk} . For our states, the three scattering lengths are close, $a_{00} : a_{01} : a_{11} = 100.4 : 97.7 : 95.0$. If the two BEC modes overlap spatially, $\phi_1 = \phi_0$, the crossed terms in (2) with the minus sign compensate the direct terms with the plus sign. Thus, by default, $\chi \approx 0$. In order to increase χ , we control the overlap of ϕ_0 and ϕ_1 with a state-dependent trapping potential. By spatially separating the two modes, the crossed terms $\partial_{N_1}\mu_0$ and $\partial_{N_0}\mu_1$ are set to zero and thus $\chi > 0$. In Fig. 1b, χ is shown as a function of the normalized density overlap $\lambda = \int dr^3 |\phi_0|^2 |\phi_1|^2 / \sqrt{\int dr^3 |\phi_0|^4 \int dr^3 |\phi_1|^4}$, calculated from stationary mode functions in traps of increasing separation for our experimental parameters (see below).

Our experimental setup is described in detail in [12] (see also Supplementary Information). In short, we use an atom chip to prepare pure BECs of $N = 1250 \pm 45$ atoms in state $|0\rangle$ in a harmonic magnetic trap with longitudinal (axial) trap frequency $f_{\text{long}} = 109$ Hz ($f_{\text{ax}} = 500$ Hz). We couple $|0\rangle$ and $|1\rangle$ with $\Omega/2\pi = 2.1$ kHz using microwave+rf radiation. The trap minima for $|0\rangle$ and $|1\rangle$ can be shifted with respect to each other along the longitudinal direction using a chip-based state-dependent microwave potential. For detection, we use state-selective absorption imaging with a carefully calibrated imaging system (see Supplementary Information). It allows us to detect both N_0 and N_1 with good accuracy in a single experimental run.

Our experimental sequence for squeezing (Fig. 1a+c) starts with a resonant $\pi/2$ -pulse of duration 120 μs to prepare the coherent spin state. During the pulse, $\Omega \gg \chi N$ so that the nonlinearity can be neglected. After the pulse, we squeeze the state by turning on χ for a well-defined time by spatially splitting and recombining the two components of the BEC in the following way (see Fig. 1c). The microwave potential is turned

on within 50 μs resulting in an abrupt separation of the trap minima for $|0\rangle$ and $|1\rangle$ by $s = 0.52$ μm . The two components of the BEC start to perform one oscillation in their respective potentials. During the oscillation, which is strongly influenced by mean-field effects, the mode functions ϕ_0 and ϕ_1 almost completely separate so that $\chi = 1.5$ s^{-1} at maximum separation. After a time $T = 12.7$ ms the states overlap again, the microwave potential is switched off within 50 μs , and the squeezing dynamics, as well as the relative atomic motion, stops. This value of T nearly coincides with the ‘best squeezing time’ expected from the two-mode model [16]. We analyze the produced state by performing state tomography. With the mean spin along x , we measure the transverse spin components $S_\theta = (\cos\theta) S_z - (\sin\theta) S_y$ along any angle θ by rotating the state vector in the yz -plane by that angle prior to detection of $S_z = (N_1 - N_0)/2$. This is done by applying a second pulse for a duration $\tau_\theta = \theta/\Omega$ and with a phase $\varphi = \pi$ ($\varphi = 0$) for turning clockwise (counterclockwise).

Figure 2a shows the noise in S_θ obtained from a large number of such measurements as a function of θ . Data for a squeezed state is shown in comparison with data for a coherent spin state where the traps were not separated during the sequence (reference measurement). We plot the normalized variance $\Delta_n S_\theta^2 = 4\Delta S_\theta^2 / \langle N \rangle$, so that $\Delta_n S_\theta^2 = 0$ dB corresponds to the standard quantum limit. In the squeezed state, the spin noise $\Delta_n S_\theta^2$ falls significantly below the standard quantum limit, reaching a minimum of $\Delta S_\theta^2 = -3.7 \pm 0.4$ dB at $\theta_{\text{min}} = 6^\circ$. The corresponding interference contrast is $C = (88 \pm 3)\%$. This results in a squeezing parameter of $\xi^2 = -2.5 \pm 0.6$ dB, proving that the state is useful for quantum metrology and that the condensate atoms are entangled. The reference measurement, by contrast, stays above the standard quantum limit for all values of θ .

Entanglement in the BEC has been defined as the non-separability of the N -particle density matrix [13, 14]. An intriguing question concerns the depth of entanglement: How large must the clusters of entangled atoms be at least in order to produce the observed squeezing? In [14], a procedure to determine the depth of entanglement from the measured spin noise reduction and mean spin length is described. Our data falls below the spin-3/2-curve in Fig. 1 of [14], which is an experimental proof that the condensate atoms are entangled in clusters of at least 4 ± 1 particles.

During the splitting, internal and motional states of the atoms are entangled. This can lead to a decrease of C and thus an increase of ξ^2 if the recombination is not perfect. To find the time of maximum contrast, we perform a Ramsey measurement where the second pulse area is $\theta = \pi/2$ and T is scanned. Figure 1d shows the resulting Ramsey fringes in the normalized population difference $N_{\text{rel}} = (N_1 - N_0)/N$ as a function of T . We observe a high contrast of $C = (88 \pm 3)\%$ at $T = 12.7$ ms,

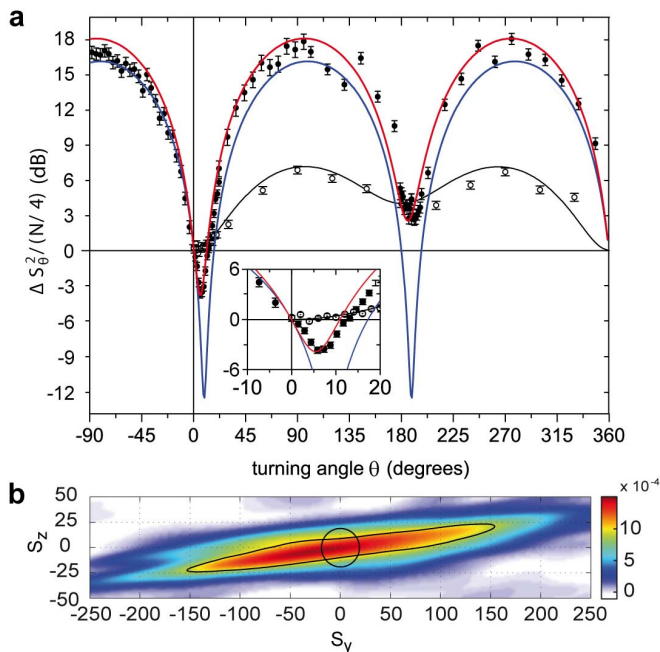


FIG. 2: **Spin noise tomography and reconstructed Wigner function of the spin-squeezed BEC.** **a**, Observed spin noise for the spin-squeezed state (solid circles) and for a coherent spin state (reference measurement, open circles). The normalized variance $\Delta_n S_\theta^2 = 4 \Delta S_\theta^2 / \langle N \rangle$ is shown as a function of the turning angle θ in the yz -plane, with statistical error bars. For this graph, we remove photon shot noise due to the imaging process as described in the Supplementary Information. In the squeezed state, a spin-noise reduction of -3.7 ± 0.4 dB is observed for $\theta_{\min} = 6^\circ$, corresponding to $\xi^2 = -2.5 \pm 0.6$ dB of metrologically useful squeezing for our Ramsey contrast of $C = (88 \pm 3)\%$. Solid lines are results from our dynamical simulation. Blue: squeezed state with losses but without technical noise; red: squeezed state with losses and technical noise; black: reference measurement with losses and technical noise. **b**, Wigner function of the spin-squeezed BEC reconstructed from our measurements. The black contour line indicates where the Wigner function has fallen to $1/\sqrt{e}$ of its maximum. Squeezed and ‘anti-squeezed’ quadratures are clearly visible. For comparison, the circular $1/\sqrt{e}$ contour of an ideal coherent spin state is shown. The area of the contour line is larger than the area of the circle indicating that the squeezed state is not a minimum uncertainty state anymore.

indicating large spatial overlap and nearly vanishing relative motion of the two states. In the squeezing sequence, we turn off the microwave potential at this time, preserving the large overlap for subsequent measurements. The contrast could be further increased using optimal control techniques [25]. In comparison with the data, we show C and λ as obtained from a simulation for our experimental parameters. For an accurate description of our system, accounting for both the spatial and the spin dynamics, we use the dynamical multi-mode theory developed in [16]. It neglects initial thermal excitations and reduces to the simple two-mode model described above for the case

of stationary condensates. The only adjustable parameter in the simulation is the splitting distance s , which is not resolved by our imaging system. The resulting value $s = 0.52 \mu\text{m}$ is consistent with a simulation of the potential. We observe very good agreement with the measurement, indicating that the simulation correctly accounts for the motion of the BEC in the trap. In Fig 1c, the simulated dynamics of the mode functions ϕ_i is shown.

The spin noise reduction obtained from this simulation is shown in Fig. 2a along with the data. We add the effect of particle loss (1,2,3-body) as determined from the two-mode Hamiltonian (1) in a Master Equation approach [16, 29], as well as several technical noise sources. The blue line shows the expected squeezing taking into account atom loss but no technical noise. The maximal reduction in variance is -12.8 dB, significantly larger than observed. The red line, which describes our data well, additionally includes the fluctuations of N , fluctuations of the pulse power of 0.5% r.m.s., a fluctuating detuning of $2\pi \times 40$ Hz r.m.s. during the pulses, and phase noise of $\Delta\varphi = 8^\circ$ r.m.s. (see Supplementary Information). All fluctuations are consistent with independent measurements. The fluctuating detuning is due to fluctuating microwave level shifts during the pulses. It is the cause for $\Delta_n S_\theta^2 > 0$ dB at $\theta = 180^\circ$. The phase noise is the main reason why the maximum achieved squeezing is smaller than the theoretically predicted value. It is consistent with technical fluctuations of the magnetic trap position in the inhomogeneous microwave near-field. Consequently, the phase noise in the reference sequence is smaller ($\Delta\varphi = 3^\circ$, black line).

The measured histograms of S_θ for different angles θ are tomographic data that allow us to reconstruct the Wigner function $W(S_y, S_z)$ of the squeezed BEC [17] using the inverse Radon transform (see Supplementary Information). Figure 2b shows the reconstruction. The two contour lines indicate where the Wigner functions of our squeezed state and of an ideal coherent spin state (with the same N and with added imaging noise) have fallen to $1/\sqrt{e}$ of their maximum. The squeezing along the direction θ_{\min} as well as the ‘anti-squeezing’ in the perpendicular direction can be clearly seen.

In conclusion, using a novel method to control interactions with a state-dependent potential, we have demonstrated for the first time spin squeezing and multi-particle entanglement on an atom chip. We envisage the implementation of this technique in portable atomic clocks and interferometers operating beyond the standard quantum limit. Furthermore, it is a valuable tool for experiments on many-body quantum physics and could enable quantum information processing on atom chips [25].

The group around M. Oberthaler has independently and simultaneously realized spin squeezing through Feshbach control of interactions in an optical trap.

-
- * E-mail: alice.sinatra@lkb.ens.fr
 † E-mail: treutlein@lmu.de; philipp.treutlein@unibas.ch
- [1] Fortágh, J. & Zimmermann, C. Magnetic microtraps for ultracold atoms. *Rev. Mod. Phys.* **79**, 235 (2007).
- [2] Hofferberth, S., Lesanovsky, I., Fischer, B., Schumm, T. & Schmiedmayer, J. Non-equilibrium coherence dynamics in one-dimensional Bose gases. *Nature* **449**, 324 (2007).
- [3] Colombe, Y. *et al.* Strong atom-field coupling for Bose-Einstein condensates in an optical cavity on a chip. *Nature* **450**, 272 (2007).
- [4] Lin, Y., Teper, I., Chin, C. & Vuletić, V. Impact of the Casimir-Polder potential and Johnson noise on Bose-Einstein condensate stability near surfaces. *Phys. Rev. Lett.* **92**, 050404 (2004).
- [5] Aigner, S. *et al.* Long-range order in electronic transport through disordered metal films. *Science* **319**, 1226–1229 (2008).
- [6] Treutlein, P., Hommelhoff, P., Steinmetz, T., Hänsch, T. W. & Reichel, J. Coherence in microchip traps. *Phys. Rev. Lett.* **92**, 203005 (2004).
- [7] Wang, Y.-J. *et al.* Atom Michelson interferometer on a chip using a Bose-Einstein condensate. *Phys. Rev. Lett.* **94**, 090405 (2005).
- [8] Schumm, T. *et al.* Matter-wave interferometry in a double well on an atom chip. *Nat. Phys.* **1**, 57 (2005).
- [9] Lloyd, S. Universal quantum simulators. *Science* **273**, 1073 (1996).
- [10] DiVincenzo, D. The physical implementation of quantum computation. *Fortschr. Phys.* **48**, 771 (2000).
- [11] Giovannetti, V., Lloyd, S. & Maccone, L. Quantum-enhanced measurements: Beating the standard quantum limit. *Science* **306**, 1330–1336 (2004).
- [12] Böhi, P. *et al.* Coherent manipulation of Bose-Einstein condensates with state-dependent microwave potentials on an atom chip. *Nat. Phys.* **5**, 592 (2009).
- [13] Sørensen, A., Duan, L.-M., Cirac, J. I. & Zoller, P. Many-particle entanglement with Bose-Einstein condensates. *Nature* **409**, 63 (2001).
- [14] Sørensen, A. & Mølmer, K. Entanglement and extreme spin squeezing. *Phys. Rev. Lett.* **86**, 4431 (2001).
- [15] Wineland, D. J., Bollinger, J. J., Itano, W. M. & Heinzen, D. J. Squeezed atomic states and projection noise in spectroscopy. *Phys. Rev. A* **50**, 67–88 (1994).
- [16] Li, Y., Treutlein, P., Reichel, J. & Sinatra, A. Spin squeezing in a bimodal condensate: spatial dynamics and particle losses. *Eur. Phys. J. B* **68**, 365–381 (2009).
- [17] Wigner, E. On the quantum correction for thermodynamic equilibrium. *Phys. Rev.* **40**, 749–759 (1932).
- [18] Rosenbusch, P. Magnetically trapped atoms for compact atomic clocks. *Appl. Phys. B* **95**, 227–235 (2009).
- [19] Estève, J., Gross, C., Weller, A., Giovanazzi, S. & Oberthaler, M. K. Squeezing and entanglement in a Bose-Einstein condensate. *Nature* **455**, 1216–1219 (2008).
- [20] Appel, J. *et al.* Mesoscopic atomic entanglement for precision measurements beyond the standard quantum limit. *Proceedings of the National Academy of Sciences* **106**, 10960–10965 (2009).
- [21] Schleier-Smith, M. H., Leroux, I. D. & Vuletić, V. Reduced-quantum-uncertainty states of an ensemble of two-level atoms. *preprint arXiv:0810.2582* (2008).
- [22] Santarelli, G. *et al.* Quantum projection noise in an atomic fountain: A high stability cesium frequency standard. *Phys. Rev. Lett.* **82**, 4619–4622 (1999).
- [23] Vogel, A. *et al.* Bose-Einstein condensates in microgravity. *Appl. Phys. B* **84**, 663 (2006).
- [24] Calarco, T. *et al.* Quantum gates with neutral atoms: Controlling collisional interactions in time-dependent traps. *Phys. Rev. A* **61**, 022304 (2000).
- [25] Treutlein, P. *et al.* Microwave potentials and optimal control for robust quantum gates on an atom chip. *Phys. Rev. A* **74**, 022312 (2006).
- [26] Charron, E., Cirone, M. A., Negretti, A., Schmiedmayer, J. & Calarco, T. Theoretical analysis of a realistic atom-chip quantum gate. *Phys. Rev. A* **74**, 12308 (2006).
- [27] Zhao, B., Chen, Z., Pan, J. & Schmiedmayer, J. High-fidelity entanglement via molecular dissociation in integrated atom optics. *Phys. Rev. A* **75**, 042312 (2007).
- [28] Kitagawa, M. & Ueda, M. Squeezed spin states. *Phys. Rev. A* **47**, 5138–5143 (1993).
- [29] Li, Y., Castin, Y. & Sinatra, A. Optimum spin squeezing in Bose-Einstein condensates with particle losses. *Phys. Rev. Lett.* **100**, 210401 (2008).
- [30] Poulsen, U. & Mølmer, K. Quantum beam splitter for atoms. *Phys. Rev. A* **65**, 33613 (2002).

Acknowledgements

It is a pleasure to thank K. Mølmer, J. Reichel, A. Smerzi, and A. Sørensen for helpful discussions and J. Halimeh for careful reading of the manuscript. This work was supported by the Nanosystems Initiative Munich. T.W.H. gratefully acknowledges support by the Max-Planck-Foundation.

Author information

Correspondence and requests for materials should be addressed to P.T. (experiment) and A.S. (simulation).

Author contributions

A.S. and P.T. jointly conceived the study. M.F.R., P.B., and P.T. carried out the experiment and analyzed the data. Y.L. and A.S. carried out the simulations. All authors discussed the results and contributed to the manuscript.

**ATOM CHIP BASED GENERATION OF ENTANGLEMENT FOR QUANTUM METROLOGY:
SUPPLEMENTARY INFORMATION**

Experimental setup

The core of our experiment is an atom chip with integrated microwave guiding structures. It allows us to generate state-dependent microwave near-field potentials in addition to static magnetic traps. The chip, the preparation of Bose-Einstein condensates (BECs), and the use of microwave near-field potentials for state-dependent coherent manipulation of ultracold atoms is described in detail in [1]. We briefly summarize it in the following, highlighting the differences to [1].

Our experimental sequence starts by preparing a BEC in state $|0\rangle$ without a discernible thermal component in a static magnetic trap on the atom chip. Magnetic shielding and the use of stable current sources ensure stable magnetic potentials which allows us to prepare BECs with well-defined total atom number $N = 1250 \pm 45$ through radio-frequency evaporative cooling. The experiment is performed in a cigar-shaped magnetic trap at a distance of $44 \mu\text{m}$ from the atom chip surface with longitudinal (axial) trapping frequency of $f_{\text{long}} = 109 \text{ Hz}$ ($f_{\text{ax}} = 500 \text{ Hz}$) and a magnetic field in the trap center of $B_0 = 3.36 \text{ G}$.

The BEC internal state is manipulated by coherently coupling the two-photon transition $|0\rangle \leftrightarrow |1\rangle$ with radio frequency and microwave radiation from an off-chip antenna and horn, respectively. The microwave is tuned $2\pi \times 360 \text{ kHz}$ above the transition to the intermediate state $|F = 2, m_F = 0\rangle$, resulting in a two-photon Rabi frequency of $\Omega = 2\pi \times 2.1 \text{ kHz}$. Fig. 3 shows the resulting Rabi oscillations for a detuning $\delta = 0$ from two-photon resonance. The efficiency of a π -pulse is $(96 \pm 1)\%$.

Figure 4a shows Ramsey interference fringes between $|0\rangle$ and $|1\rangle$ as a function of the delay T between two $\pi/2$ -pulses. This is a reference measurement taken in a static magnetic trap without splitting the condensate, i.e. with the BEC in a coherent spin state. The Ramsey contrast at $T = 12.7 \text{ ms}$ is $C = (96 \pm 1)\%$. While the pulses are applied, the two-photon resonance frequency is shifted by $\Delta_{\text{mw}} = 2\pi \times 7.6 \text{ kHz}$ with respect to the undriven system. This is due to differential AC Zeeman level shifts of $|0\rangle$ and $|1\rangle$ caused by the detuned microwave radiation of the two-photon drive [2]. We always adjust the frequency of the two-photon drive such that the detuning from two-photon resonance is $\delta = 0$ while the pulse is applied. In between the pulses, the phase of the atomic superposition state thus evolves at a rate $-\Delta_{\text{mw}}$ with respect to the two photon drive. This determines the frequency of the Ramsey oscillations in Fig. 4a.

For state-selective spatial splitting and recombination of the two BEC components, we use a microwave near-field potential created with an on-chip waveguide. Compared with [1], the detuning of the microwave near-field

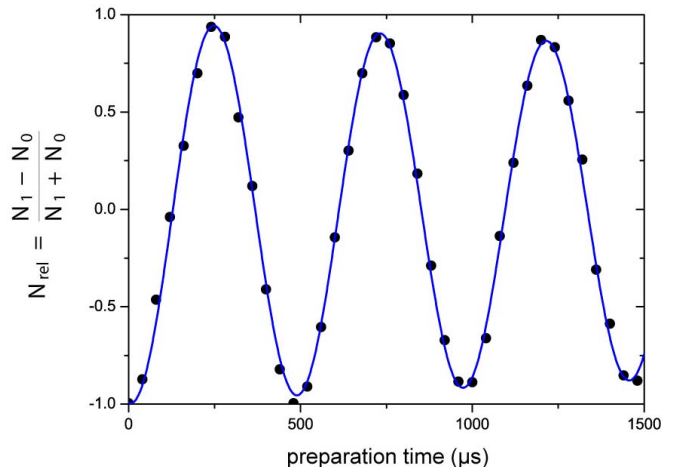


FIG. 3: **Rabi oscillations.** Resonant Rabi oscillations of the relative atom number $N_{\text{rel}} = (N_1 - N_0)/(N_1 + N_0)$ recorded by varying the duration of the state preparation pulse. The efficiency of a π -pulse is $(96 \pm 1)\%$. The decay with a time constant of 15 ms is due to gradients in Ω near the structured metallic chip surface which imposes boundary conditions on the electromagnetic field.

from the transition $|F = 1, m_F = 0\rangle \leftrightarrow |F = 2, m_F = 0\rangle$ is much larger, $2\pi \times 12 \text{ MHz}$, so that admixtures of other states to $|0\rangle$ and $|1\rangle$ are smaller and the states are more robust against magnetic field noise. In this configuration, both states experience a microwave potential of opposite sign, and with different magnitude due to the different hyperfine transition strengths. At a microwave power of $P_{\text{mw}} = 120 \text{ mW}$ launched into the chip, a splitting of the potential minima for the two states of $s = 0.52 \mu\text{m}$ results.

Figure 4b shows Ramsey fringes measured in the squeezing sequence, i.e. the BEC is split and recombined during the time T between the $\pi/2$ -pulses as in Fig. 1 of the main text. Turning on the microwave near-field potential has two effects: The oscillation frequency of the Ramsey fringes slightly decreases because of the differential energy shift experienced by the two states in the potential. More importantly, the fringe contrast is modulated by the overlap of the BEC mode functions ϕ_0 and ϕ_1 . The contrast at $T = 12.7 \text{ ms}$, the time at which the squeezed state is analyzed in the experiment, determines the length of the mean collective spin: $C = 2|\langle S_x \rangle|/N$. We observe a contrast of $C = (88 \pm 3)\%$, smaller than in the reference because the overlap of the BEC mode functions after splitting and recombination is less than unity. The difference to the contrast predicted by the dynamical simulation of 94% can most likely be explained by small motion in the transverse direction which is excited in the experiment but not modeled. The contrast could be in-

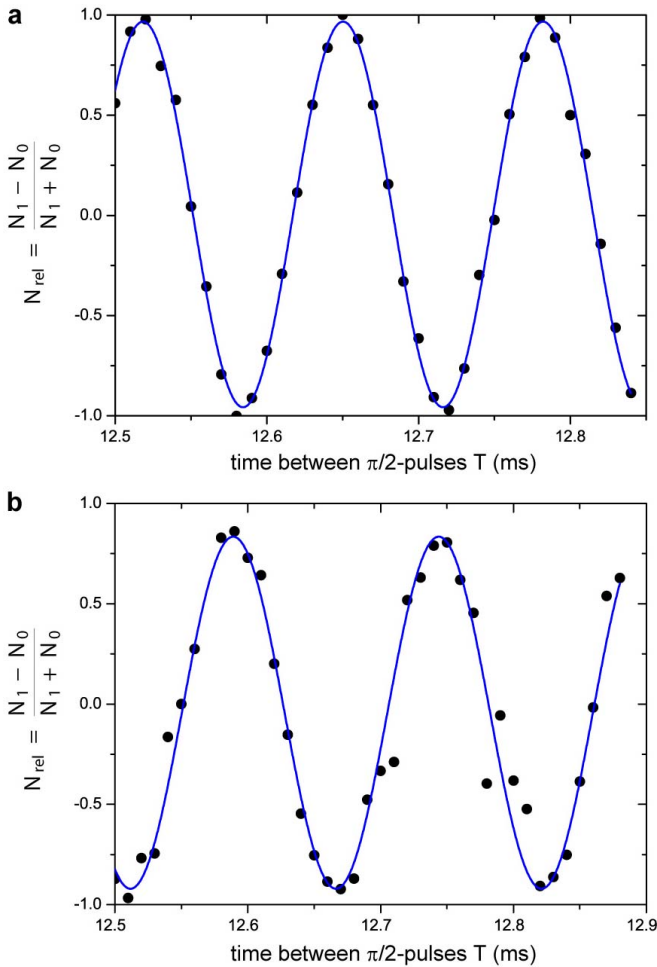


FIG. 4: **Ramsey interference fringes.** Ramsey interference fringes in the relative atom number N_{rel} recorded by varying the delay T between two $\pi/2$ -pulses. **a**, Ramsey fringes in the reference sequence in a static magnetic trap. The contrast obtained from a sinusoidal fit is $C = (96 \pm 1) \%$. **b**, Ramsey fringes in the squeezing sequence with state-selective splitting and recombination of the BEC embedded between the $\pi/2$ -pulses, as in Fig. 1d of the main text. The contrast is $C = (88 \pm 3) \%$.

created by optimal control of the atomic motion rather than abrupt switching of the potentials, as described in [25].

Imaging system

Compared with [1], we use an improved detection system which allows us to take absorption images of both states and determine N_0 and N_1 in a single shot of the experiment. We use a back-illuminated deep-depletion CCD camera with a quantum efficiency of 90% at 780 nm and fast line transfer. After the squeezing sequence described in the main text, the atoms are transferred within 30 ms into a relaxed trap with $f_{\text{long}} = 40$ Hz and

$f_{\text{ax}} = 130$ Hz at a distance of 200 μm from the chip surface. The trap is switched off and states $|1\rangle$ and $|0\rangle$ are imaged after times-of-flight of 4.6 ms and 6.1 ms, respectively. State $|1\rangle$ is directly imaged with a σ^- -polarized resonant laser beam on the $F = 2 \rightarrow F' = 3$ cycling transition. After the image is taken, atoms in $|1\rangle$ fly out of the depth of focus of the imaging system due to the photon recoil momentum transferred during the imaging pulse. Subsequently, state $|0\rangle$ is optically pumped into the $F = 2$ manifold of the ground state using a $F = 1 \rightarrow F' = 2$ pumping laser [3] and imaged on the $F = 2 \rightarrow F' = 3$ transition. For both states, the imaging pulse duration is 40 μs and the imaging intensity is $I = 0.8 I_{\text{sat}}$, where I_{sat} is the saturation intensity on the cycling transition. The FWHM diameters of the imaged atom clouds are 15 μm in the vertical and 10 μm in the horizontal direction, both larger than the optical resolution of our imaging system of 4 μm . The maximum optical densities in the cloud centers for 600 atoms in each state are 1.2 and 1.4, respectively. The good agreement of the observed Rabi oscillations with the expected sinusoidal behavior proves the linearity of our imaging system.

For the correct determination of the fluctuations of S_θ it is crucial to know the total atom number $N = N_0 + N_1$ accurately. We calibrate our imaging system by two independent methods. First, following the method of [4], we adjust the effective scattering cross section σ_{eff} which is used to calculate the atom number from the optical density of the cloud such that the measured atom number is independent of the imaging light intensity. We find $\sigma_{\text{eff}} = 0.9 \sigma_0$, where σ_0 is the theoretically expected scattering cross section on the $|F = 2, m_F = -2\rangle \leftrightarrow |F' = 3, m_F' = -3\rangle$ cycling transition. This is plausible taking into account optical pumping in the beginning of the imaging pulse and imperfect imaging light polarization.

An independent test of this calibration can be obtained by observing the scaling of projection noise with total atom number for a coherent spin state. Figure 5 shows the variance ΔS_z^2 measured directly after a $\pi/2$ -pulse as a function of the total atom number N . The constant offset due to imaging noise is subtracted as described below. The observed linear behavior confirms that projection noise $\Delta S_z^2 \propto N$ dominates over technical noise which generically scales as $\Delta S_z^2 \propto N^2$. If we use the first method to calibrate N , a fit to the data in Fig. 5 with a straight line through the origin yields a slope of 0.22 ± 0.01 . This agrees with the theoretically expected slope of 1/4 to better than 15%. The difference lies within the error bar of our atom number calibration according to the first method. As the dependence of ΔS_z^2 on N can be very accurately determined from Fig. 5, we use it to calibrate the total atom number by rescaling N so that the slope of the linear fit is 1/4.

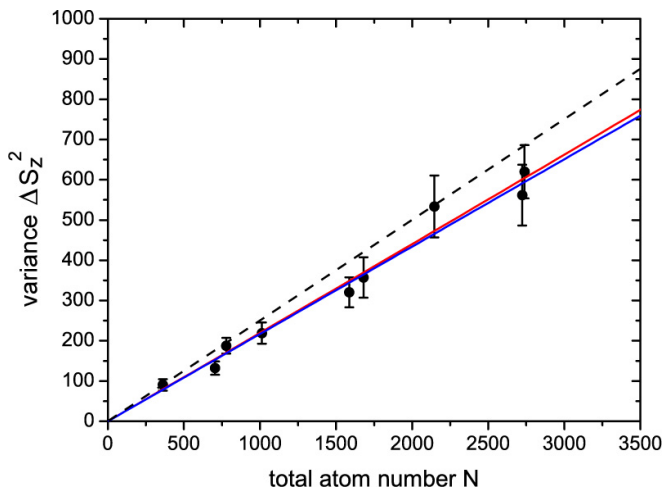


FIG. 5: **Projection noise as a function of atom number.** A measurement of the variance ΔS_z^2 directly after a $\pi/2$ -pulse is shown as a function of total atom number N , where N is independently calibrated with the method of [4]. The dashed line shows the expected linear scaling with a slope of $1/4$, the blue line is a linear fit to the data which yields a slope of 0.22 ± 0.01 . The red line is a quadratic fit with $\Delta S_z^2 = aN + bN^2$. It yields $a = 0.22 \pm 0.02$ and $b = (0.06 \pm 1) \times 10^{-5}$, confirming the linear scaling expected for projection noise.

Data evaluation

Our experiment runs very stable and we can usually let it record data overnight without supervision. The data shown in Fig. 2 of the main text is gathered during 7 measurement nights with between 80 (for $20 < \theta < 90$) and 370 (for $0 < \theta < 20$) experimental realizations per point. The error bars are statistical errors assuming a normal distribution.

We analyze the recorded images by counting atoms in the two states within two small rectangular regions with a typical size of $30 \mu\text{m} \times 30 \mu\text{m}$. This yields N_0 and N_1 and thus $S_z = (N_1 - N_0)/2$. Only shots where the total atom number N differs by no more than 150 from the mean $N = 1250$ are used for the analysis and we check that a tighter (75 atoms) or wider (250 atoms) post-selection does not significantly change the data quality. In the data for $90^\circ < \theta < 360^\circ$ a slow drift of $N_1 - N_0$ is observed. We correct for this technical drift by subtracting a filtered data set from the respective raw data, using a second order Savitzky-Golay filter [5] over 300 shots.

In Fig. 2a of the main text, we additionally correct ΔS_z^2 for noise in our imaging system. Photon shot noise from the imaging beam contributes to the measured fluctuations of N_0 and N_1 with a standard deviation of $\Delta N_{0,\text{psn}}$ and $\Delta N_{1,\text{psn}}$, respectively. We determine this noise either by measuring the apparent atom number fluctuations in regions of the image where no atoms are present, by taking ‘reference shots’ where no atoms are prepared in the first place, or by calculating the expected shot noise from

the observed imaging light intensity. All methods yield similar results. We correct the variance of S_z as

$$\Delta S_{z,\text{corr}}^2 = \Delta S_z^2 - (\Delta N_{0,\text{psn}}^2 + \Delta N_{1,\text{psn}}^2)/4.$$

The applied correction due to imaging noise corresponds to typically $(\Delta N_{0,\text{psn}}^2 + \Delta N_{1,\text{psn}}^2)^{1/2}/2 \approx 7$ atoms. Finally, we normalize the variance to the expected variance for a coherent spin state with $\langle N_0 \rangle = \langle N_1 \rangle = \langle N \rangle/2$, obtaining $\Delta_n S_z^2 = 4 \Delta S_{z,\text{corr}}^2 / \langle N \rangle$. Without subtraction of imaging noise, we still observe a reduction in the spin fluctuations of -2.3 dB.

Phase noise

In our experiment, phase noise is the main reason why we do not reach the theoretically predicted spin noise reduction. It is therefore important to identify and eliminate the main technical sources for this noise. In the squeezing sequence with $\theta = 6^\circ$, where we observe the minimum of ΔS_θ^2 , we measure the dependence of S_θ on various experimental parameters. From this we can calculate the sensitivity of the relative phase between the atomic state and our two-photon drive on these parameters. We independently determine the technical fluctuations of these parameters and estimate their contribution to the total phase noise of $\Delta\varphi = 8^\circ$. Timing jitter of our experiment control (≈ 100 ps), fluctuations of the external magnetic field (reduced by a μ -metal shield to ≈ 0.3 mG), power fluctuations ($\approx 5 \times 10^{-3}$) and phase instabilities ($\approx 0.3^\circ$) of the radio frequency and microwave generators and amplifiers for the two-photon drive, and fluctuations of the on-chip currents together contribute a phase noise of about 1° . The microwave power coupled into the on-chip waveguide for creating the near-field potential fluctuates by $60 \mu\text{W}$ (5×10^{-4}) leading to a phase noise of 2° . The remaining phase noise is consistent with fluctuations of a current source used to create a magnetic field for the static magnetic trap. Its effect on the phase is not due to the small differential magnetic moment between $|0\rangle$ and $|1\rangle$ but due to a shift of the magnetic trap position in the highly inhomogeneous microwave near-field which leads to fluctuating microwave level shifts.

Wigner Function reconstruction

We reconstruct the Wigner function of the spin-squeezed condensate in the following way: For each measured $\theta \in [-90^\circ, 90^\circ]$ we create a histogram of S_θ and fit it with a cubic spline to obtain a smooth curve. We then use a filtered back-projection algorithm [6] to perform an inverse Radon transform [7]. The inverse Radon transform is derived for classical image reconstruction in a plane. In [8], it has been used to reconstruct the Wigner

function of squeezed states of the electromagnetic field. However, it is generally not suited to reconstruct an arbitrary spin state on the curved Bloch sphere. In our case the spin-squeezed state does not ‘wrap around’ the Bloch sphere so that we can locally approximate the Bloch sphere by a plane and use the inverse Radon transform. We furthermore make a continuum approximation to the measured values of S_z , which is reasonable as our imaging system does not have single atom resolution. With the experimental method presented here but with a more sophisticated analysis [9], the density matrix of arbitrary spin states that spread over the whole Bloch sphere can be reconstructed. Quantum state tomography is of interest as it gives access to measures of entanglement such as the quantum Fisher information [10, 11], which characterizes a more general class of states (including states with $\xi^2 > 1$) that can be used to overcome the standard quantum limit [11].

* E-mail: alice.sinatra@lkb.ens.fr

† E-mail: treutlein@lmu.de; philipp.treutlein@unibas.ch

- [1] Böhi, P. *et al.* Coherent manipulation of Bose-Einstein condensates with state-dependent microwave potentials on an atom chip. *Nat. Phys.* **5**, 592 (2009).
 [2] Gentile, T., Hughey, B., Kleppner, D. & Ducas, T. Ex-

- perimental study of one- and two-photon Rabi oscillations. *Phys. Rev. A* **40**, 5103 (1989).
 [3] Matthews, M. R. *et al.* Dynamical response of a Bose-Einstein condensate to a discontinuous change in internal state. *Phys. Rev. Lett.* **81**, 243 (1998).
 [4] Reinaudi, G., Lahaye, T., Wang, Z. & Guéry-Odelin, D. Strong saturation absorption imaging of dense clouds of ultracold atoms. *Opt. Lett.* **32**, 3143–3145 (2007).
 [5] Savitzky, A. & Golay, M. Smoothing and differentiation of data by simplified least squares procedures. *Analytical Chemistry* **36**, 1627–1639 (1964).
 [6] Natterer, F. *The Mathematics of Computerized Tomography* (Society for Industrial & Applied Mathematics, U.S., 1986).
 [7] Radon, J. Über die Bestimmung von Funktionen durch ihre Integralwerte längs gewisser Mannigfaltigkeiten. *Berichte Sächsische Akademie der Wissenschaften* **29**, 262–279 (1917).
 [8] Breitenbach, G., Schiller, S. & Mlynek, J. Measurement of the quantum states of squeezed light. *Nature* **387**, 471–475 (1997).
 [9] D’Ariano, G. M., Maccone, L. & Painsi, M. Spin tomography. *J. Opt. B: Quantum Semiclass. Opt.* **5**, 77–84 (2003).
 [10] Frieden, B. R. & Soffer, B. H. Lagrangians of physics and the game of Fisher-information transfer. *Physical Review E* **52**, 2274–2286 (1995).
 [11] Pezzé, L. & Smerzi, A. Entanglement, nonlinear dynamics, and the Heisenberg limit. *Phys. Rev. Lett.* **102**, 100401 (2009).